



# Multi-objective crashworthiness optimization of tapered thin-walled tubes with axisymmetric indentations

E. Acar<sup>a</sup>, M.A. Guler<sup>a,\*</sup>, B. Gerçeker<sup>a</sup>, M.E. Cerit<sup>a</sup>, B. Bayram<sup>b</sup>

<sup>a</sup> Department of Mechanical Engineering, TOBB University of Economics and Technology, Söğütözü, Ankara 06560, Turkey

<sup>b</sup> TEMSA AR-GE VE TEKNOLOJİ A.Ş., Tübitak MAM Teknoloji Serbest Bölgesi içi, Gebze, Kocaeli 41470, Turkey

## ARTICLE INFO

### Article history:

Received 22 February 2010

Received in revised form

21 August 2010

Accepted 22 August 2010

Available online 17 September 2010

### Keywords:

Crush force efficiency

Specific energy absorption

Finite element analysis

LS-DYNA

Surrogate models

Multi-objective optimization

Axisymmetric indentation

Taper

Tubes

## ABSTRACT

In this paper, the effects of tapering and introducing axisymmetric indentations on the crash performances of thin-walled tubes are investigated. The crash performances of the tubes are evaluated using two metrics: the crush force efficiency (CFE, the ratio of the average crushing load to the peak load), and the specific energy absorption (SEA, absorbed energy per unit mass). The optimum values of the number of the axisymmetric indentations, the radius of the indentations, the taper angle and the tube thickness are sought for maximum CFE and maximum SEA using surrogate based optimization. In addition, multi-objective optimization of the tubes is performed by maximizing a composite objective function that provides a compromise between CFE and SEA. The CFE and SEA values at the training points of surrogate models (metamodels) are computed using the finite element analysis code LS-DYNA. Polynomial response surfaces, radial basis functions, and Kriging are the different surrogate models used in this study. Surrogate based optimization of the tubes showed that the tubes with indentations have better crush performance than tubes without indentations. It is found that maximum CFE requires large number of indentations with high radius, small thickness, and medium taper angle, while maximum SEA requires small number of indentations with low radius, large thickness and small taper angle. It is also found that the globally most accurate surrogate model does not necessarily lead to the optimum.

© 2010 Elsevier Ltd. All rights reserved.

## 1. Introduction

The driver and passenger safety are crucial elements in design of automotive structures. The main goal of the designers in the automotive industry is to design crashworthy vehicles. Energy absorbing elements (e.g., shotguns, side rails) are mainly responsible for providing the safety of both the passengers and the critical vehicle components. These elements convert the crash energy into strain energy through structural deformation. Although many different types of energy absorbers exist, the thin-walled tubes are the most common energy absorbing elements.

Crushing behavior of thin-walled tubes has been investigated by many researchers. These studies have mainly focused on tubes with cylindrical and square cross-sections [1,2], while other types of cross-sections are also investigated [3]. The tubes can be straight or tapered. For straight tubes, the tube side-walls are parallel to the tube axis. The straight tubes tend to buckle, which reduces the energy absorbing capability [4]. Therefore, tapered

tubes are preferred over straight tubes, since they provide constant mean load-deflection response and are good at withstanding oblique impacts as well as axial loads [5]. The energy absorption characteristics of tapered tubes under impact loading were investigated by Nagel and Thambiratnam [6]. They studied the effect of the number of tapered sides and the wall thickness on the energy absorption behavior. In addition to tapering the tubes, several other design strategies have been suggested in literature including introducing geometrical discontinuities or imperfections in the form of indentations, grooves, dents, holes corrugations [7–15]. All these aforementioned studies have been focused on analyzing the effect of tapering or geometrical discontinuities only. This paper aims to analyze the effect of tapering and geometrical discontinuities on the crash performance of tubes.

The crush forces generated during the axial impact is one of the important parameters to be considered in designing the energy absorbers. For an energy absorber, it is not sufficient to maximize the absorbed energy, but the amount of the crush force must also be decreased for the safety of both the passengers and the crashworthiness of the vehicle components. The initial peak crush force should be reduced as much as possible. Therefore, both peak crush force and energy absorption values should be

\* Corresponding author. Tel.: +90 312 292 4088; fax: +90 312 292 4091.  
E-mail address: [mguler@etu.edu.tr](mailto:mguler@etu.edu.tr) (M.A. Guler).

investigated in determining the efficiency of a crush absorber. For example, Jin and Altenhof [16] studied the efficiency of the round and square extrusions under a cutting deformation by calculating the crush force efficiency (CFE) and specific energy absorption (SEA). CFE can be defined as the ratio of the mean crush force to the peak crush force. SEA may be defined as the energy absorption per unit mass, which is an important parameter for the applications in which the weight of the structure is also crucial. Therefore, specific energy absorption value should be controlled and the energy absorber should be examined with respect to its weight efficiency [17].

The main objective of this study is to investigate the effect of various geometrical parameters such as wall thickness, semi-apical angle (i.e., taper angle), and properties of geometrical discontinuities on the energy absorption characteristics of thin-walled structures. This analysis can be performed using experimental and numerical techniques. Since experiments are expensive and time consuming, finite element simulations are generally used in automotive industry. In this study, a commercially available explicit dynamic finite element (FE) analysis code LS-DYNA [18] is used to simulate the collapse behavior of the thin-walled tubes under axial impact loading. The finite element models were validated by the previously established solutions from literature, which allowed several designs to be analyzed without having to build and test several prototypes.

In this study, the optimum values of the geometrical parameters and the properties of geometrical discontinuities are

sought for maximum crush force efficiency and maximum specific energy absorption. The main challenge in crashworthiness optimization is the extremely high computational costs of crash simulations. To overcome the computational challenge, researchers have focused on using surrogate models (or metamodels) that can mimic the behavior of the simulation model as closely as possible while being computationally very efficient to evaluate. Crashworthiness optimization for whole vehicles or their components using surrogate models has been performed by several researchers (e.g., [19–26]). Focusing mainly on energy absorption performances of thin-walled tubes, Refs. [27–33] used surrogate models to perform crashworthiness optimization of the tubes. In this study, surrogate based optimization of the tubes are performed to determine the optimum values of the number of the axisymmetric indentations, the radius of the indentations, the taper angle and the tube thickness for maximum CFE and maximum SEA. In addition; multi-objective optimization of the tubes is performed by maximizing a composite objective function that provides a compromise between CFE and SEA.

The paper is structured as follows. The next section provides the problem description of the crash performance optimization of the tapered thin-walled tubes with axisymmetric indentations. Section 3 presents the details of the finite element analysis of the tubes. Section 4 discusses surrogate model construction. The results of the optimization problem are given in Section 5, followed by the concluding remarks given in Section 6.

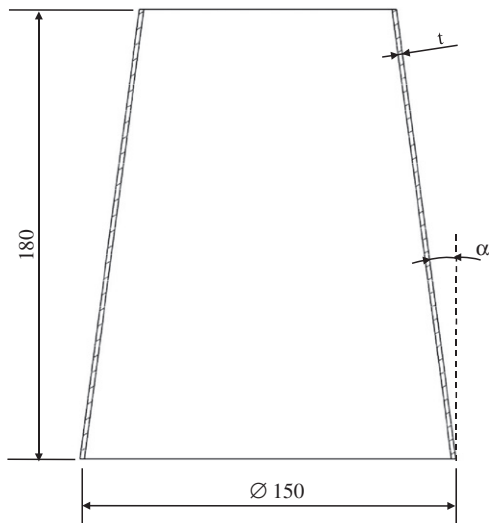


Fig. 1. The geometry of the thin walled tube (without axisymmetric indentations) having circular cross-section. The dimensions are in millimeters.

## 2. Problem description

The thin-walled tubes having circular cross sections have been modeled with and without axisymmetric indentations as shown in Figs. 1 and 2, respectively. The tubes have a largest diameter of 150 mm, and a length of 180 mm. For the crash performance of tubes, the following design problem is considered. The tubes are impacted with a 1500 kg rigid wall with an initial velocity of 9 m/s (see Fig. 3). This would generate an initial kinetic energy of 45 kJ in accordance with ECE R-29 requirements for trucks.

The tubes should be designed for maximum crash performance, which is evaluated by two metrics (CFE and SEA). The variables that can be tailored by a designer are chosen as the followings: (1) the tube wall thickness,  $t$ ; (2) the taper angle, ( $\alpha$ ); (3) the radius of axisymmetric indentations,  $R_i$ ; and (4) the number of indentations,  $N_i$ . Thus, optimization problem for maximum CFE (or maximum SEA) can be stated as

Find  $t, \alpha, N_i, R_i$

Min -CFE(or-SEA)

Such that  $1 \text{ mm} \leq t \leq 2.5 \text{ mm}$

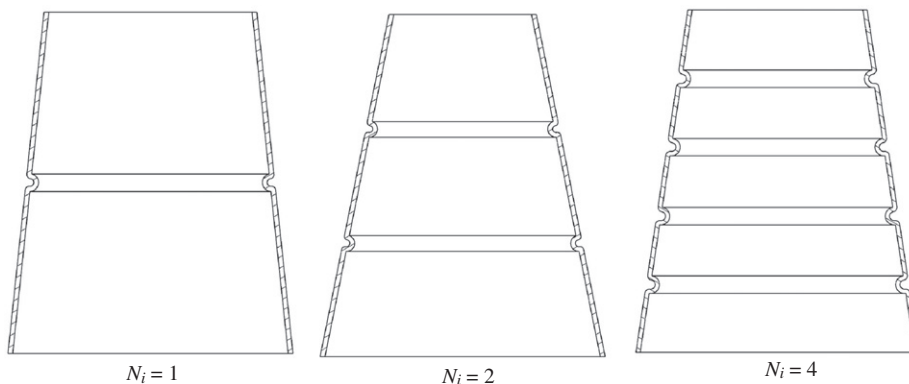


Fig. 2. The geometry of the thin walled tube (with axisymmetric indentations) having circular cross-section.

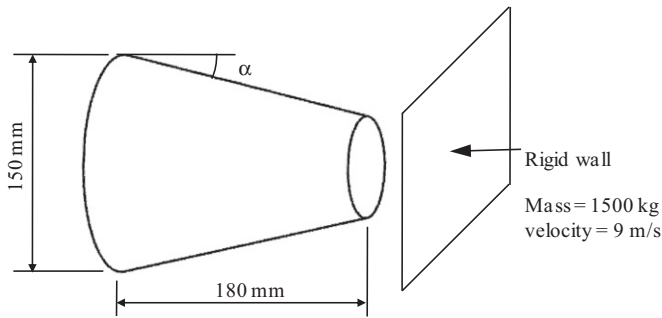


Fig. 3. The tube impacted with a rigid wall.

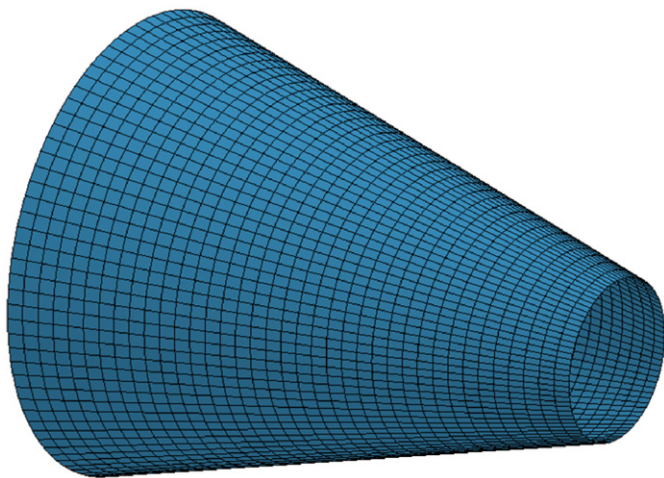


Fig. 4. Finite element mesh of the tubes without indentations.

$$\begin{aligned} 0 &\leq \alpha \leq 15^\circ \\ 1 &\leq N_i \leq 5 \\ 3 \text{ mm} &\leq R_i \leq 9 \text{ mm} \end{aligned} \quad (1)$$

Instead of maximizing for either CFE or SEA, a multi-objective optimization problem can be formulated by defining a composite objective function that can provide a compromise between CFE and SEA. The composite objective function to be maximized can be defined as

$$f = w \frac{\text{CFE}}{\text{CFE}_0} + (1-w) \frac{\text{SEA}}{\text{SEA}_0} \quad (2)$$

where  $f$  is the composite objective function to be maximized,  $w$  is a weight factor used to adjust the relative importance CFE and SEA to each other, and  $\text{CFE}_0$  and  $\text{SEA}_0$  are the normalization constants for the CFE and SEA, respectively. Here, the values of these normalization constants are taken as the maximum CFE and SEA values obtained at the training points.

The optimization problems defined in this section are solved by using “*fmincon*” built-in function of MATLAB [34] that uses sequential quadratic programming. To ensure the global convergence, the optimization runs used 100 different starting points.

### 3. Finite element simulations

The finite element crash simulations of this study have been performed by using explicit, nonlinear finite element code LS-DYNA. Thin walled tubes were fixed at one end and impacted

Table 1

True stress–true plastic strain values for mild steel.

$\sigma_r$ (MPa)	331	347	390	427	450	469	501	524	533	533
$\epsilon_p$	0	0.018	0.0374	0.056	0.075	0.093	0.138	0.18	0.23	0.5

by a rigid wall having an initial velocity of 9 m/s and a mass of 1500 kg in axial direction. The schematic of the finite element mesh is shown in Fig. 4.

The finite element models of the tubes are created by using the commercial pre-processor software ANSA [35]. The size of the quadrilateral elements is chosen to be  $5 \times 5 \text{ mm}^2$ . The tubes are modeled with 4-noded Belytschko–Lin–Tsay shell elements having five integration points through the thickness. Belytschko–Lin–Tsay shell element is used, because it requires less mathematical calculations compared to other types of shell elements.

The material models used are the “Material type 20 rigid material” for the rigid wall and the “Material type 24 elasto-plastic material.” For Material type 24, the plastic region is included with true stress–true strain curve. Mild steel properties are used for the tubes. Poisson’s ratio, density and Young’s modulus are taken as 0.3,  $7850 \text{ kg/m}^3$  and 210 GPa, respectively. True stress and true plastic strain values for mild steel are shown in Table 1. Strain rate effects are included in the elasto-plastic material definition, where the strain rate parameters  $C$  and  $P$  for the mild steel in the Cowper–Symonds model are taken 0.04 1/s and 5, respectively, as in earlier studies [36,37].

For contact definitions, “automatic single surface” contact algorithm is used. The self-contact of the tubes, and the contact between the tube and the rigid wall are defined by using this type of contact. The static and dynamic friction coefficients for the tubes are taken as 0.3 and 0.2, respectively. The friction coefficient between the tube and the moving rigid wall is taken to be 0.3. Comparison of the FE model results for frusta with those from previously established solutions [6,12] is provided in Table 2.

### 4. Constructing surrogate models

When calculation of the responses that appear in the objective function or constraint function formulations requires computationally expensive simulations, optimizing the design becomes challenging. In such conditions, surrogate models can offer a practical remedy. Surrogate models aim at regression and/or interpolation fitting of the response data at some specified training points that are selected using one of the many designs of experiments (DOE) techniques given the bounds on the input variables. By computing the responses at the training points, a corresponding pool of response values is generated. Then, the matrix of input and output values are used to fit a surrogate model, which in turn can be used to estimate the value of response at any arbitrary point within the bounds of the input variables.

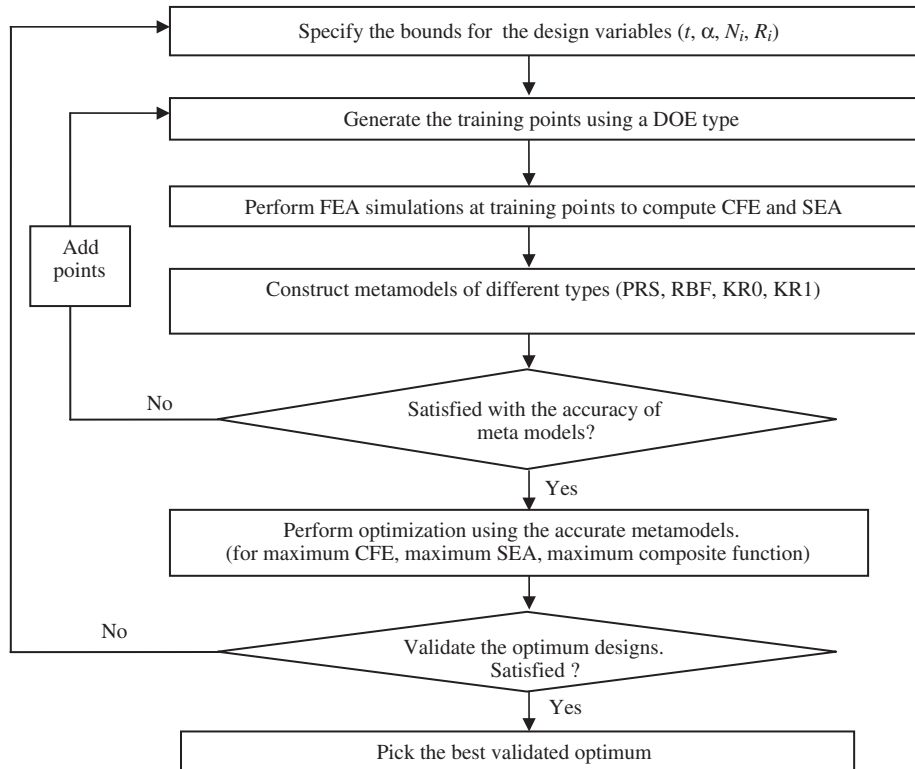
#### 4.1. Design of experiments

The first step of constructing a surrogate model is to select a DoE type. Two main families of design of experiments exist [38]: (i) classic designs and (ii) space filling designs. The most commonly used classic experimental designs include fractional factorial design (FFD), central composite design (CCD) and Box–Behnken designs [38]. Popular space filling designs include maximum entropy designs [39], minimax and maximin designs [40], Latin hypercube sampling (LHS) designs [41] and orthogonal arrays [42]. In this study, FFD design of experiments is used for

**Table 2**

Comparison of the FE model results for frusta with those from previously established solutions [6,12].

		Semi-apical angle, $\alpha$ (deg)			
		5	7.5	10	14
Nagel and Thambiratnam [6]	Crush distance (mm)	87.97	88.30	84.30	98.56
	Total energy absorption (kJ)	1.08	2.42	2.40	2.29
Mamalis et al. [12]	Crush distance (mm)	89.50	83.50	89.00	90.50
	Total energy absorption (kJ)	1.04	2.67	2.50	2.07
Present study	Crush distance (mm)	88.57	84.36	80.64	95.2
	Total energy absorption (kJ)	1.08	2.45	2.52	2.24

**Fig. 5.** Flowchart for performing surrogate-based optimization of the tubes.

the tubes without indentations and LHS design of experiments is used for the tubes with indentations. Brief details of these DoEs are provided in Appendix A.

#### 4.2. Surrogate models

After selecting the DoE type (that is, determining the locations of the training points), the CFE and SEA values at the training points are computed using LS-DYNA. Next, different types of surrogate models are constructed using the DoE information and the computed CFE and SEA values. Polynomial response surface (PRS) approximations, radial basis functions (RBF) and Kriging (KR) models are used as different types of surrogate models. A brief overview of the mathematical formulation of PRS, RBF and KR is provided in Appendix B. Then, the constructed surrogate models are used for optimization. Finally, the surrogate model predictions at the optimum tube configurations are validated using LS-DYNA. A flowchart showing the steps followed while

performing surrogate-based optimization of the tubes is shown in Fig. 5.

### 5. Optimization results

In this section, the optimization results for designs with and without axisymmetric indentations are provided. The optimum results obtained using different surrogate models are compared. Finally, FEA of the optimum designs are performed to check surrogate model predictions.

#### 5.1. Tubes without axisymmetric indentations

For the tubes without axisymmetric indentations, tube wall thickness ( $t$ ) and taper angle ( $\alpha$ ) are used as design variables. These design variables are the input variables for the surrogate models. The lower and upper bounds of these input variables are specified as  $1 \text{ mm} \leq t \leq 2.5 \text{ mm}$ , and  $0^\circ \leq \alpha \leq 15^\circ$ , respectively.

Full factorial design with three levels is used to generate training points (Table 3, columns 2 and 3). Then, FEA simulations are performed to compute CFE and SEA at the training points (Table 3, columns 4 and 5).

Second-order PRS (PRS2), RBF, and Kriging models with zeroth- and first-order trend models (KRO and KR1) are constructed for CFE and SEA prediction. The constructed surrogate models are depicted in Figs. 6 and 7. Notice that RBF, KRO and KR1 surrogate models pass through all training points, while PRS2 does not.

The accuracies of the constructed surrogate models are evaluated using leave-one-out generalized mean square cross validation error metric, GMSE. The GMSE is calculated as follows. If there are  $N$  training points, a surrogate model type is constructed  $N$  times, each time leaving out one of the training points. Then, the difference between the exact value of the response  $y^k$  at the omitted training point  $\mathbf{x}_k$  and the predicted value of the response using the surrogate model is calculated. Finally, GMSE is calculated from

$$\text{GMSE} = \frac{1}{N} \sum_{k=1}^N (y^k - \hat{y}^{(k)})^2 \quad (3)$$

Table 4 provides the comparison of the GMSE of the surrogate models. Also, the GMSE values are normalized with respect to the

**Table 3**

Training points and responses evaluated. The maximum CFE and SEA at the training points is depicted in bold fonts.

No.	Taper angle, $\alpha$ (deg)	Thickness, $t$ (mm)	CFE	SEA (Kj/kg)
1	0.0	1.00	0.1674	9.17
2	0.0	1.75	0.2726	14.89
3	0.0	2.50	0.3439	18.54
4	7.5	1.00	0.2440	10.70
5	7.5	1.75	0.3697	16.60
6	7.5	2.50	<b>0.4559</b>	<b>20.64</b>
7	15.0	1.00	0.2890	10.20
8	15.0	1.75	0.3787	14.19
9	15.0	2.50	0.3368	19.52

GMSE of the most accurate model, and given in Table 4. It is seen from Table 4 that the RBF model is the most accurate model for the CFE prediction, while KR1 is the most accurate model for the SEA prediction.

Then, optimization for maximum CFE is performed using each surrogate model separately. Table 5 lists the optimum tube configurations (see columns 2 and 3) and CFE predictions (see column 4) by surrogate models. Amongst the four optimum configurations obtained, three of them (namely RBF, KRO, KR1) are very close to the 6th training point having a CFE value of 0.4559. Thus, no extra FEA is required for a confirmation run. This CFE value will be compared to the optimum CFE value of the tubes with axisymmetric indentations in Section 5.2 to evaluate the effect of introducing indentations on CFE of the tubes.

Then, optimization for maximum SEA is performed using each surrogate model separately. The optimum tube configurations (see columns 2 and 3) and SEA predictions (see column 4) are provided in Table 6. It is found that the optimum SEA value corresponding to all surrogate models are close to that of the 6th training point (20.64). Again, no extra FEA is required for a confirmation run. This SAE value will be compared to the optimum SEA value of the tubes with axisymmetric indentations in Section 5.2 to evaluate the effect of introducing indentations on SEA of the tubes.

Instead of optimizing the tubes for either maximum CFE or maximum SEA, the tubes are also optimized for the composite objective function (see Eq. (2)) that provides a compromise between the CFE and SEA. We consider the case when CFE and SEA are equally important, so the weight factor in Eq. (2) is taken as  $w=0.5$ . The values of  $\text{CFE}_0$  and  $\text{SEA}_0$  in Eq. (2) are taken as 0.4559 and 20.64, respectively, corresponding to the maximum CFE and SEA evaluated at the data points (see Table 3). The optimization results are listed in Table 7. Since the maximization of CFE and SEA both yielded optima close to the 6th training point, it is not surprising to find that the maximization of the composite objective function also yields optimum values close to the 6th training point.

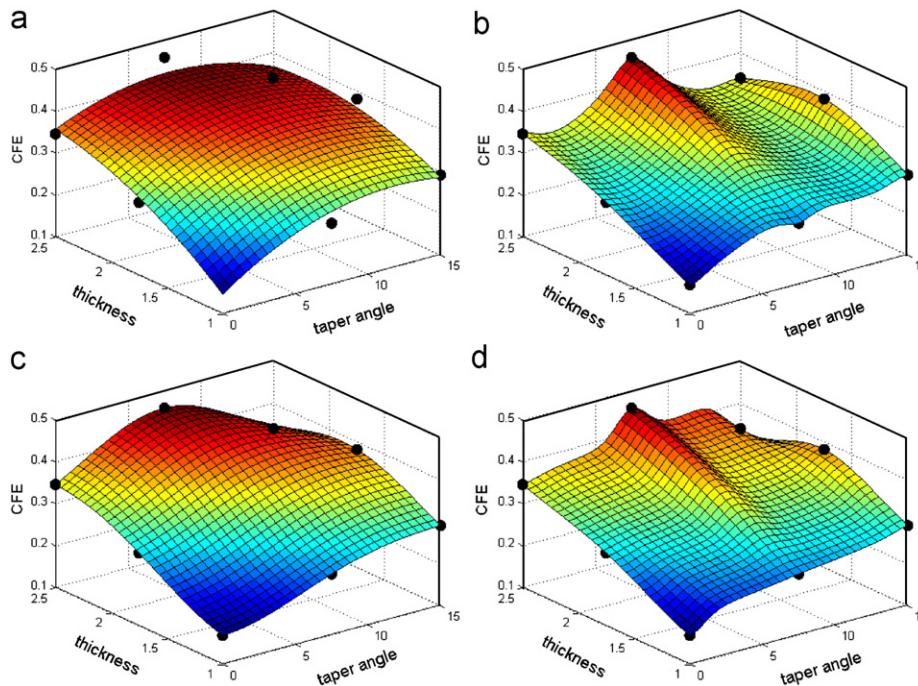


**Fig. 6.** Constructed surrogate models for CFE prediction. The bold black dots in the plots show the training points: (a) PRS2, (b) RBF, (c) KRO and (d) KR1.

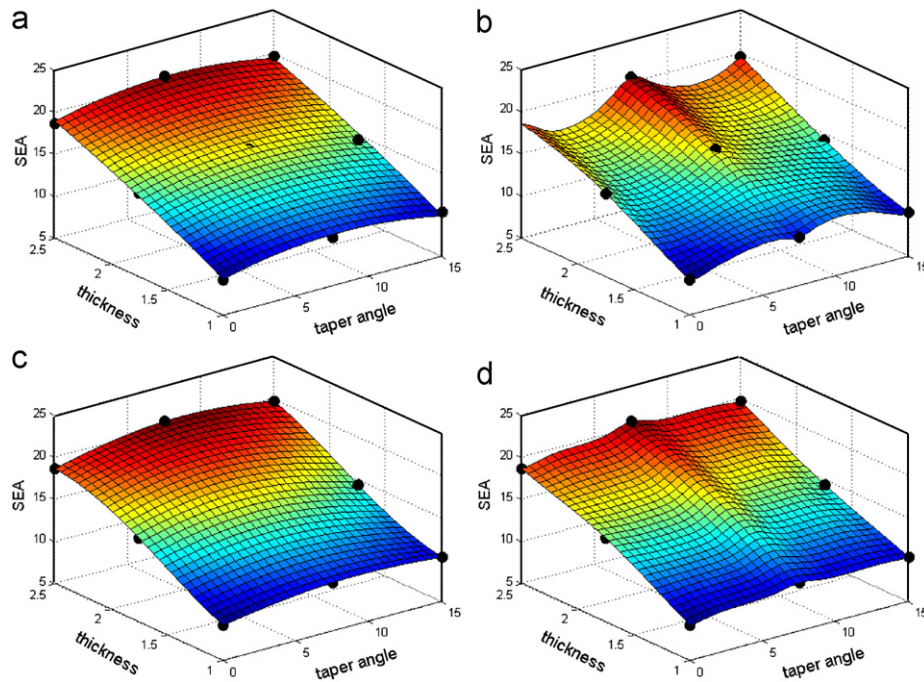


Fig. 7. Constructed surrogate models for SEA prediction. The bold black dots in the plots show the training points. (a) PRS2; (b) RBF; (c) KRO; (d) KR1.

Table 4

Accuracies of different surrogate models constructed for CFE and SEA predictions for the tubes *without* indentations.

	PRS2	RBF	KRO	KR1
<i>Accuracies of surrogate models for CFE prediction</i>				
Generalized mean square cross validation errors	0.076	0.065	0.085	0.070
Errors normalized with respect to the most accurate	1.17	<b>1.00</b>	1.32	1.08
<i>Accuracies of surrogate models for SEA prediction</i>				
Generalized mean square cross validation errors	1.30	1.75	2.96	1.10
Errors normalized with respect to the most accurate	1.19	1.60	2.70	<b>1.00</b>

Table 5

Optimization results for the tubes *without* indentations for maximum CFE.

Surrogate model	$\alpha$ (deg)	$t$ (mm)	CFE prediction
PRS2	7.79	2.5	0.4180
RBF	7.50	2.5	0.4559
KRO	7.39	2.5	0.4560
KR1	7.57	2.5	0.4561

Table 6

Optimization results for the tubes *without* indentations for maximum SEA.

Surrogate model	$\alpha$ (deg)	$t$ (mm)	SEA prediction
PRS2	7.99	2.5	20.62
RBF	7.57	2.5	20.65
KRO	8.76	2.5	20.69
KR1	7.55	2.5	20.65

## 5.2. Tubes with axisymmetric indentations

For the tubes with axisymmetric indentations, the number of indentations ( $N_i$ ) and the indentation radius ( $R_i$ ) are used as additional design variables along with the tube wall thickness ( $t$ ) and taper angle ( $\alpha$ ). These four variables are the input variables

for the surrogate models, and their lower and upper bounds are provided in Table 8.

LHS design of experiments is used to generate 81 training points, and PRS2, RBF, KRO and KR1 surrogate models are constructed. Then, the accuracies of surrogate models for CFE and SEA prediction are compared. Table 9 shows that the most accurate surrogate model for CFE is RBF, while the most accurate surrogate model for SEA is KR1 as in the case of the tubes *without* indentations.

First, optimization for maximum CFE is performed using each surrogate model separately. The optimum tube configurations (see columns 2 through 5) and CFE predictions are provided in Table 10. Notice that the maximum CFE of the tubes with indentations (0.8017) is 76% larger than the maximum CFE obtained for the tubes *without* indentations (0.4559).

Next, optimization for maximum SEA is performed using each surrogate model separately. The optimum tube configurations (see columns 2 through 5) and SEA predictions (see column 6) are provided in Table 11. Notice that the maximum SEA of the tubes with indentations (22.45) is only 9% larger than the maximum SEA of the tubes *without* indentations (20.64). This shows that introducing axisymmetric indentations is more effective for increasing CFE than SEA.

Then, the optimization of the tubes is performed to maximize the composite objective function of CFE and SEA (see Eq. (2)). The weight factor in Eq. (2) is taken as  $w=0.5$ , and the values of  $CFE_0$  and  $SEA_0$  used in Eq. (2) are taken as 0.7715 and 21.16,

**Table 7**Optimization results for tubes the tubes *without* indentations for maximum composite objective function with  $w=0.5$ .

Surrogate model	$\alpha$ (deg)	$t$ (mm)	CFE prediction	SAE prediction	Composite objective function prediction
PRS2	7.87	2.5	0.4180	20.62	0.958
RBF	7.53	2.5	0.4559	20.65	1.000
KR0	7.62	2.5	0.4558	20.65	1.000
KR1	7.57	2.5	0.4561	20.65	1.000

**Table 8**Lower and upper bounds of the design variables for the tubes *with* axisymmetric indentations.

	$\alpha$ (deg)	$t$ (mm)	$N_i$	$R_i$ (mm)
Lower bound	0	1.0	1	3.0
Upper bound	15	2.5	5	9.0

**Table 9**Accuracies of different surrogate models constructed for CFE and SEA prediction for tubes *with* axisymmetric indentations.

	PRS2	RBF	KR0	KR1
<i>Accuracies of surrogate models for CFE prediction</i>				
Generalized mean square cross validation errors	0.076	0.073	0.081	0.082
Errors normalized with respect to the most accurate	1.04	<b>1.00</b>	1.11	1.12
<i>Accuracies of surrogate models for SEA prediction</i>				
Generalized mean square cross validation errors	0.863	0.792	0.794	0.623
Errors normalized with respect to the most accurate	1.39	1.27	1.28	<b>1.00</b>

**Table 10**Optimization results for the tubes *with* axisymmetric indentations for maximum CFE.

Surrogate model	$\alpha$ (deg)	$t$ (mm)	$N_i$	$R_i$ (mm)	CFE prediction
PRS2	10.00	1	5	3	0.7258
RBF	8.684	2.255	4	4.672	<b>0.8017</b>
KR0	9.975	1.684	4	4.582	0.7895
KR1	10.01	1.656	4	4.457	0.7835

**Table 11**Optimization results for the tubes *with* axisymmetric indentations for maximum SEA.

Surrogate model	$\alpha$ (deg)	$t$ (mm)	$N_i$	$R_i$ (mm)	SEA prediction
PRS2	0	2.5	1	3	22.39
RBF	6.023	2.5	1	4.088	22.45
KR0	3.788	2.302	1	4.114	21.61
KR1	4.473	2.5	1	3.298	22.30

**Table 12**Optimization results for the tube *with* axisymmetric indentations for maximum composite objective function with  $w=0.5$ .

Surrogate model	$\alpha$ (deg)	$t$ (mm)	$N_i$	$R_i$ (mm)	Composite objective function prediction
PRS2	6.576	2.5	1	3.827	0.8455
RBF	11.38	2.5	2	3.625	0.9707
KR0	9.926	2.136	2	3.879	0.9314
KR1	6.023	2.176	2	3.465	0.9389

respectively. These values (that is, CFE=0.7715 and SEA=21.16) correspond to the maximum CFE and SEA values evaluated at the data points. The optimization results are listed in Table 12. It is seen that RBF model provides the largest composite objective function prediction.

The optimum tube configurations leading to the maximum CFE, the maximum SEA, and the maximum composite objective functions are depicted in Fig. 8. It is seen that the number of indentations and taper angle are large for maximum CFE, while a single indentation with small taper angle is required for maximum

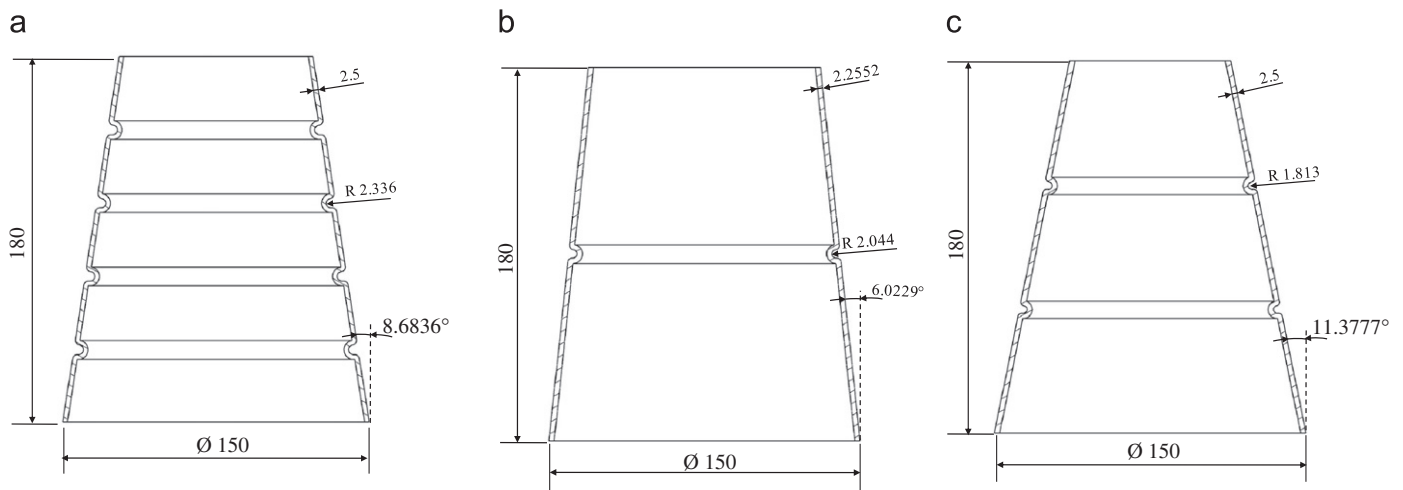


Fig. 8. The geometry of the thin walled tube for (a) maximum CFE, (b) maximum SEA, and (c) maximum composite objective function with  $w=0.5$ .

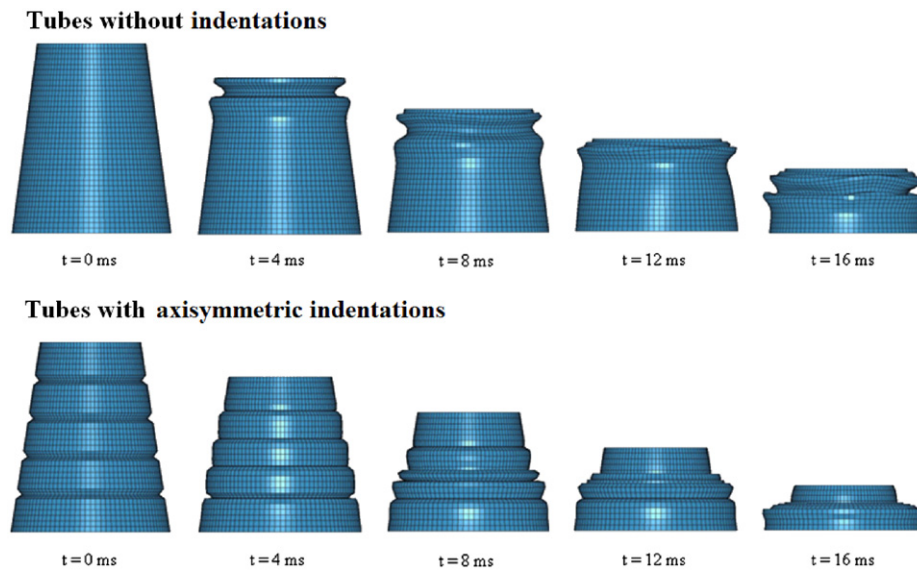


Fig. 9. Crash behavior of the tubes with and without indentations.

SEA. A compromised configuration can be achieved by having two indentations with a larger taper angle. The crash behaviors of the tubes with and without indentations for maximum CFE are shown in Fig. 9, which shows the superiority of the tubes with indentations over the tubes without indentations in terms of CFE.

Finally, Pareto optimal sets for the tubes with indentations are obtained by solving the multi-objective optimization problem for various values of the weight factor  $w$  in Eq. (2) between 0 and 1. The Pareto optimal fronts obtained using different surrogate models are depicted in Fig. 10. It is seen that the Pareto front of PRS2 is shallow, while the other fronts are sharp, showing a clear knee point.

### 5.3. Checking performances of surrogate based optima using FEA

In this section, FEA simulations of the optimum tube configurations obtained using surrogate based optimization are performed to compute the actual performances of the tubes.

Recall that the prediction of the maximum CFE of the tubes with indentations was 0.8017, while the FE analyses show that the maximum CFE is 0.7923 (see Table 13). Comparing this value to the maximum CFE obtained for the tubes without indentations

(0.4559), it is seen that the CFE improvement due to introducing indentations is 74%. It is also seen that the tube configuration with maximum CFE is obtained from KR0, even though RBF model provided the maximum CFE predictions as well as RBF was the most accurate surrogate model for CFE prediction.

Similarly, the prediction of the maximum SEA of the tubes with indentations was 22.45, while the FE analyses show that the maximum CFE is 22.22. Comparing this value to the maximum CFE obtained for tubes without indentations (20.64), it is seen that the CFE improvement due to introducing indentations is 8%. It is seen that even though KR1 was the most accurate model for SEA prediction, the tube configuration with maximum SAE is obtained from RBF. The overall conclusion is that the globally most accurate surrogate model does not necessarily lead to the optimum design.

## 6. Conclusion

Crash performances of the thin-walled tubes with and without axisymmetric indentations were optimized in this paper. The design variables were selected as the number of indentations, the radius of the indentations, the taper angle and the tube thickness.

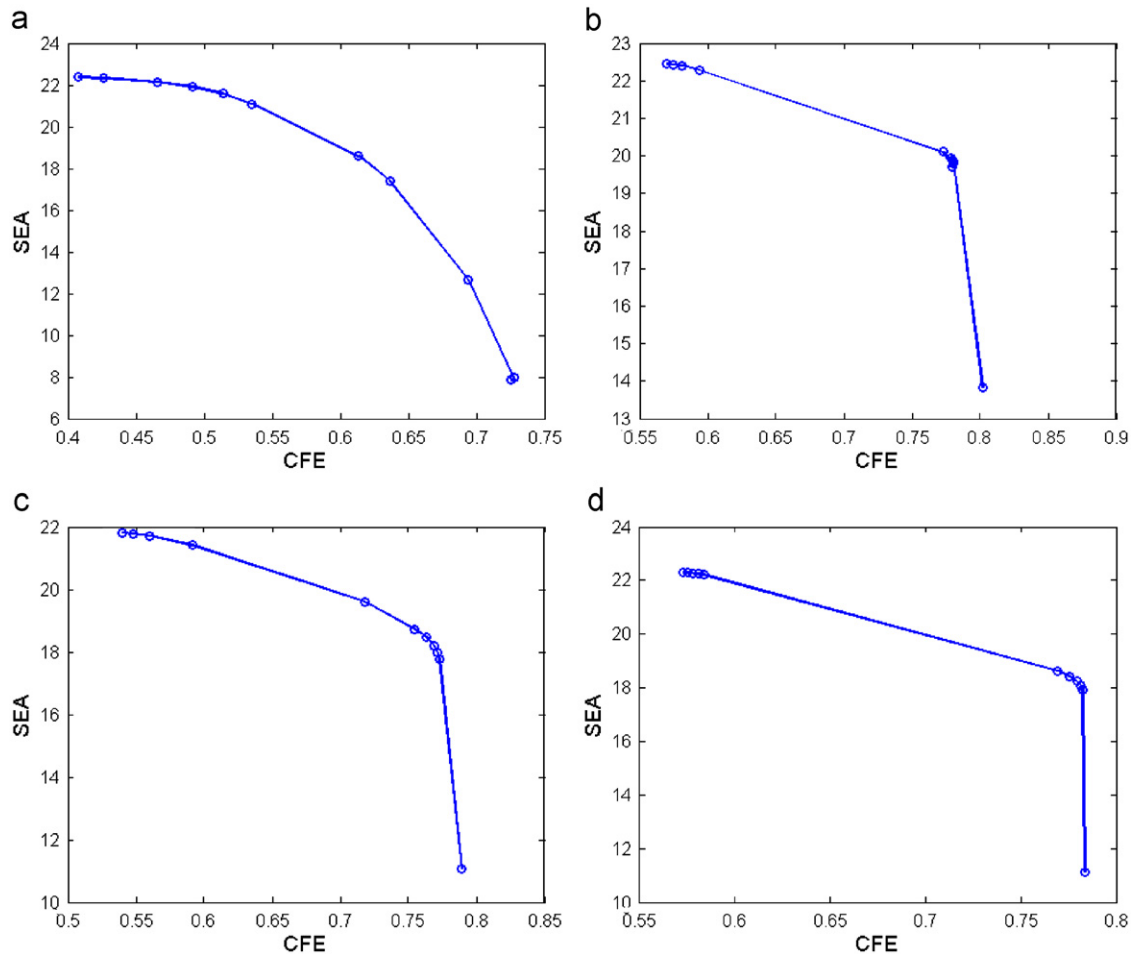


Fig. 10. The Pareto optimal fronts obtained using different surrogate models.

Table 13

Finite element analysis of the optimum tube configurations obtained via surrogate based optimization.

Maximize for	Surrogate model predictions			Finite element analysis results		
	CFE	SEA	Composite	CFE	SEA	Composite
<i>Evaluating performance of PRS2</i>						
CFE	0.7258	7.85	0.6559	0.7099	8.34	0.6572
SEA	0.4077	22.39	0.7933	0.4507	17.90	0.7151
Composite	0.5314	21.20	0.8455	0.6809	22.12	<b>0.9640</b>
<i>Evaluating performance of RBF</i>						
CFE	<b>0.8017</b>	13.84	0.8467	0.7125	9.93	0.6964
SEA	0.5698	<b>22.45</b>	0.8999	0.6051	<b>22.22</b>	0.9173
Composite	0.7793	19.70	<b>0.9707</b>	0.6916	17.94	0.8722
<i>Evaluating performance of KR0</i>						
CFE	0.7895	11.09	0.7737	<b>0.7923</b>	14.61	0.8588
SEA	0.5402	21.61	0.8608	0.6348	20.67	0.9001
Composite	0.7545	18.73	0.9314	0.7871	18.82	0.9548
<i>Evaluating performance of KR1</i>						
CFE	0.7835	11.13	0.7709	0.7708	11.97	0.7824
SEA	0.573	22.30	0.8983	0.5724	22.07	0.8927
Composite	0.7694	18.63	0.9389	0.7882	18.90	0.9575

The specific energy absorption, SEA, and crush force efficiency, CFE, of the tubes were optimized using surrogate models. In addition, multi-objective optimization of the tubes was performed by maximizing a composite objective function that

provides a compromise between CFE and SEA. From the results obtained in this study, the following conclusions were drawn:

- For both the tubes with and without indentations, RBF was found to be the most accurate surrogate model for CFE prediction, while KR1 was the most accurate surrogate model for SEA prediction.
- The maximum CFE obtained for the tubes with indentations was 76% larger than the maximum CFE obtained for the tubes without indentations based on the surrogate model predictions. The validation of the optimum tube configurations via FEA showed that the actual improvement of CFE was 74%.
- The maximum SEA obtained for the tubes with indentations was only 9% larger than the maximum SEA obtained for the tubes without indentations based on the surrogate model predictions. The validation of the optimum tube configurations via FEA revealed that the actual increase of SEA was 8%.
- Overall, introducing indentations was found to be more effective for improving CFE than SEA.
- Maximum CFE required large number of indentations, small thickness, and medium taper angle, while maximum SEA requires small number of indentations, large thickness and small taper angle.
- Even though RBF was the most accurate model for CFE prediction, the tube configuration with maximum CFE is obtained from KR0. Similarly, although KR1 was the most accurate model for SEA prediction, the tube configuration with maximum SAE is obtained from RBF. So, we concluded that the

globally most accurate surrogate model does not necessarily lead to the optimum design.

**Acknowledgments**

This study is funded by the Turkish Ministry of Industry and Trade and TEMSA ARGE VE TEKNOLOJI A.S. within the scope of the SAN-TEZ project 00236.STZ.2008-1.

**Appendix A. Brief details of FFD and LHS design of experiments**

In this study, FFD is used for the tubes without indentations and LHS is used for the tubes with indentations. Brief details of these designs of experiments are provided below.

**A.1. Full factorial design**

Full factorial design consists of two or more factors, each with discrete possible values or “levels”, and whose experimental units take on all possible combinations of these levels across all factors (variables). When  $k$  number of levels is used for  $n$  variables, the total number of experiments is  $k^n$ . If there are three variables and two-levels are used for all variables, then the total number of experiments is eight as shown in Fig. A1. In this study, three-level designs are used for both two and four variable cases.

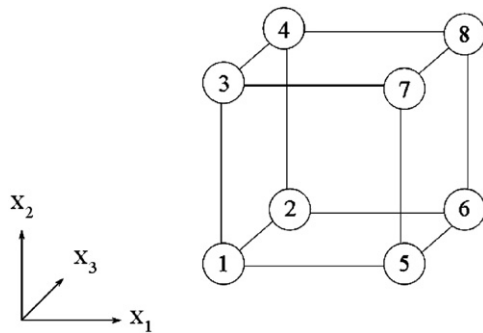


Fig. A1. Full factorial design for three variables with two levels.

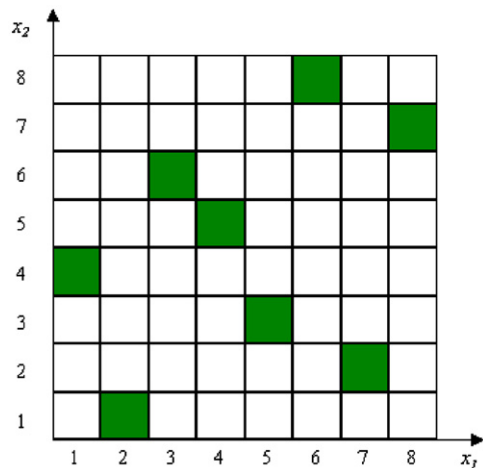


Fig. A2. Latin hypercube sampling for two design variables with eight design points.

**A.2. Latin hypercube sampling**

In the LHS method, the range of values for each variable is divided into  $m$  segments of equal probability. The whole design space consisting of  $n$  variables is partitioned into  $m^n$  cells each having equal probability. For example, for the case of two variables and eight segments, the design space is divided into 64 cells as illustrated in Fig. A2. The next step is to choose  $m$  cells as design points from the  $m^n$  cells. First, a random sample is generated, and its cell number is calculated. The cell number indicates the segment number the sample belongs to, with respect to each of the variables. For example, a cell number (2, 1) indicates that the sample lies in Segment 2 with respect to the first variable and in Segment 1 with respect to second variable. At each successive step, a random sample is generated and is accepted only if it does not agree with any previous sample on any of the segment numbers with respect to each of the variables. The shaded cells in Fig. A2 are the final selected design points.

**Appendix B. Surrogate models used**

In this study, polynomial response surface approximations (PRS), radial basis functions (RBF) and Kriging (KR) models are used as different types of surrogate models. A brief overview of the mathematical formulation of these surrogate models taken from [43] is provided in the followings.

**B.1. Polynomial response surface (PRS) approximations**

The most commonly used PRS model is the second-order model in the form of a second-degree algebraic polynomial function as [44]

$$\hat{f}(x) = b_0 + \sum_{i=1}^L b_i x_i + \sum_{i=1}^L b_{ii} x_i^2 + \sum_{i=1}^{L-1} \sum_{j=i+1}^L b_{ij} x_i x_j \tag{B.1}$$

where  $\hat{f}$  is the response surface approximation of the actual response function,  $f$ ,  $L$  is the number of variables in the input vector  $\mathbf{x}$ , and  $b_0, b_i, b_{ii}, b_{ij}$  are the unknown coefficients to be determined by the least squares technique.

**B.2. Radial basis functions (RBF)**

RBF methods were originally developed to approximate multi-variate functions based on scattered data [45]. For a data set consisting of the values of input variables and response values at  $n$  sampling points, the true function  $f(\mathbf{x})$  can be approximated as

$$\tilde{f}(\mathbf{x}) = \sum_{i=1}^n \lambda_i \phi(\|\mathbf{x} - \mathbf{x}_i\|) \tag{B.2}$$

where  $\mathbf{x}$  is the vector of input variables,  $\mathbf{x}_i$  is the vector of input variables at the  $i$ th sampling point,  $\|\mathbf{x} - \mathbf{x}_i\| = \sqrt{(\mathbf{x} - \mathbf{x}_i)^T (\mathbf{x} - \mathbf{x}_i)}$  is the Euclidean norm representing the radial distance,  $r$  from design point  $\mathbf{x}$  to the sampling point or center  $\mathbf{x}_i$ ,  $\phi$  is a radially symmetric basis function, and  $\lambda_i, i = 1, n$  are the unknown interpolation coefficients. Eq. (B.2) represents a linear combination of a finite number of radially symmetric basis functions. Some of the most commonly used RBF formulations include:  $\phi(r) = r^2 \log(r)$  (thin-plate spline);  $\phi(r) = e^{-\alpha r^2}, \alpha > 0$  (Gaussian);  $\phi(r) = \sqrt{r^2 + c^2}$  (multiquadric); and  $\phi(r) = 1/\sqrt{r^2 + c^2}$  (inverse multiquadric). The parameter  $c$  in the multiquadrics is a constant. If the  $r$  values are normalized to the

range of (0,1), then  $0 < c \leq 1$ . The choice of  $c = 1$  is found to be suitable for most function approximations. The feature that makes these functions excellent candidates for  $\phi$  is not simply their radial symmetry but their smoothness and certain properties of their Fourier transform [44]. In this study, we have chosen the multi-quadric formulation of RBF because of its prediction accuracy and its commonly linear and possibly exponential rate of convergence with increased sampling points.

Given the design coordinates of  $n$  sampling points and associated responses, the unknown coefficients in Eq. (B.2) are found by minimizing the residual or the sum of the squares of the deviations expressed as

$$R = \sum_{j=1}^n \left[ f(\mathbf{x}_j) - \sum_{i=1}^n \lambda_i \phi(\|\mathbf{x}_j - \mathbf{x}_i\|) \right]^2 \quad (\text{B.3})$$

Expressed in matrix form, Eq. (B.3) appears as

$$[A]\{\lambda\} = \{f\} \quad (\text{B.4})$$

where  $[A] = [\phi\|\mathbf{x}_j - \mathbf{x}_i\|]$ ,  $j = 1, n$ ,  $i = 1, n$ ;  $\{\lambda\}^T = \{\lambda_1, \lambda_2, \dots, \lambda_n\}^T$ , and  $\{f\}^T = \{f(x_1), f(x_2), \dots, f(x_n)\}^T$ . The coefficient vector  $\lambda$  is obtained by solving Eq. (B.4).

### B.3. Kriging (KR)

The basic assumption of KR is the estimation of the response in the form

$$f(x) = p(x) + Z(x) \quad (\text{B.5})$$

where  $f$  is the response function of interest,  $p$  is a known polynomial that globally approximates the response, and  $Z(x)$  is the stochastic component that generates deviations such that the Kriging model interpolates the sampled response data. The stochastic component has a mean value of zero and covariance

$$\text{COV}[Z(x_i), Z(x_j)] = \sigma^2 \mathbf{R}[R(x_i, x_j)] \quad (\text{B.6})$$

where  $\mathbf{R}$  is  $N \times N$  correlation matrix if  $N$  is the number of training points,  $R(x^i, x^j)$  is correlation function between the two training points  $x^i$  and  $x^j$ . Mostly, the correlation function is chosen as Gaussian, that is,

$$R(\theta) = \prod_{k=1}^L \exp(-\theta_k d_k^2) \quad (\text{B.7})$$

where  $L$  is the number of variables,  $d_k = x_k^i - x_k^j$  is the distance between the  $k$ th components of the two training points  $x^i$  and  $x^j$ , and  $\theta_k$  are the unknown parameters to be determined.

Once the correlation function has been selected, the response  $f$  is predicted as

$$\hat{f}(x) = \hat{\beta} + \mathbf{r}^T(x) \mathbf{R}^{-1} (\mathbf{f} - \hat{\beta} \mathbf{p}) \quad (\text{B.8})$$

where  $\mathbf{r}^T(x)$  is the correlation vector of length  $N$  between a prediction point  $x$  and the  $N$  sampling points,  $f$  represents the responses at the  $N$  points and  $p$  is an  $L$ -vector of ones (in the case that  $p(x)$  is taken as a constant). The vector  $\mathbf{r}$  and scalar  $\hat{\beta}$  are given by

$$\mathbf{r}^T(x) = [R(x, x^1), R(x, x^2), \dots, R(x, x^N)]^T, \quad \hat{\beta} = (\mathbf{p}^T \mathbf{R}^{-1} \mathbf{p})^{-1} \mathbf{p}^T \mathbf{R}^{-1} \mathbf{f} \quad (\text{B.9})$$

The variance of the output model (which is different than the variance of the sampled output) can be estimated as

$$\hat{\sigma}^2 = \frac{(\mathbf{f} - \hat{\beta} \mathbf{p})^T \mathbf{R}^{-1} (\mathbf{f} - \hat{\beta} \mathbf{p})}{N} \quad (\text{B.10})$$

The unknown parameters  $\theta_k$  can be estimated by solving the following constrained maximization problem [46]

$$\begin{aligned} \text{Max } \Phi(\Theta) &= \frac{-[N \ln(\hat{\sigma}^2) + \ln |\mathbf{R}|]}{2} \\ \text{s.t. } \Theta &> 0 \end{aligned} \quad (\text{B.11})$$

where  $\Theta$  is the vector of unknown parameters  $\theta_k$ , and both  $\hat{\sigma}$  and  $\mathbf{R}$  are functions of  $\Theta$ . In this work, we use a MATLAB Kriging toolbox developed by Lophaven et al. [47].

### References

- [1] Langseth M, Hopperstad OS. Static and dynamic axial crushing of square thin-walled aluminum extrusions. *Int J Impact Eng* 1996;18:949–68.
- [2] Hsu SS, Jones N. Quasi-static and dynamic axial crushing of thin-walled circular stainless steel, mild steel and aluminium alloy tubes. *Int J Crashworthiness* 2004;9(2):195–217.
- [3] Najafi A, Rais-Rohani M. Influence of cross-sectional geometry on crush characteristics of multi-cell prismatic columns. In: 49th AIAA/ASME/ASCE/AHS/ASC structures, structural dynamics, and materials conference, Schaumburg, IL, April 2008.
- [4] Gupta NK, Easwara Prasad GL, Gupta SK. Plastic collapse of metallic conical frusta of large semi-apical angles. *Int J Crashworthiness* 1997;2:349–66.
- [5] Reid SR, Reddy TY. Static and dynamic crushing of tapered sheet metal tubes of rectangular cross-section. *Int J Mech Sci* 1986;28:623–37.
- [6] Nagel GM, Thambiratnam DP. Dynamic simulation and energy absorption of tapered tubes under impact loading. *Int J Crashworthiness* 2004;9(4):389–99.
- [7] Hosseini-pour SJ, Daneshi GH. Energy absorption and mean crushing load of thin-walled grooved tubes under axial compression. *Thin-Walled Struct* 2003;41(1):31–46.
- [8] Lee S, Hahn C, Rhee M, Oh J. Effect of triggering on the energy absorption capacity of axially compressed aluminum tubes. *Mater Des* 1999;20:31–40.
- [9] Singace AA, El-Sobky H. Behavior of axially crushed corrugated tubes. *Int J Mech Sci* 1997;39(3):249–68.
- [10] Elgalai AM, Mahdi E, Hamouda AMS, Sahari BS. Crushing response of composite corrugated tubes to quasi-static axial loading. *Compos Struct* 2004;66:665–71.
- [11] Guler MA, Cerit ME, Bayram B, Gerçeker B, Karakaya E. The effect of geometrical parameters on the energy absorption characteristics of thin-walled structures under axial impact loading. *Int J Crashworthiness*, in press, doi:10.1080/13588260903488750.
- [12] Mamalis AG, Manolakos DE, Ioannidis MB, Kostazos PK, Hassiotis G. Finite element simulation of the axial collapse of thin-wall square frusta. *Int J Crashworthiness* 2001;6(2):155–64.
- [13] Karbhari VM, Chaoling X. Energy absorbing characteristics of circular frusta. *Int J Crashworthiness* 2003;8(5):471–8.
- [14] Mamalis AG, Manolakos DE, Spentzas KN, Ioannidis MB, Koutroubakis S, Kostazos PK. The effect of the implementation of circular holes as crush initiators to the crushing characteristics of mild steel square tubes: experimental and numerical simulation. *Int J Crashworthiness* 2009;14(5):489–501.
- [15] Arnold B, Altenhof W. Experimental observations on the crush characteristics of AA6061 T4 and T6 structural square tubes with and without circular discontinuities. *Int J Crashworthiness* 2004;9(1):73–87.
- [16] Jin SY, Altenhof W. Comparison of the load/displacement and energy absorption performance of round and square AA6061-T6 extrusions under a cutting deformation mode. *Int J Crashworthiness* 2007;12(3):265–78.
- [17] Liu Y. Design optimisation of tapered thin-walled square tubes. *Int J Crashworthiness* 2008;13(5):543–50.
- [18] LS-DYNA keyword user's manual, version 970, Livermore Software Corporation, 2004.
- [19] Forsberg J, Nilsson L. Evaluation of response surface methodologies used in crashworthiness optimization. *Int J Impact Eng* 2006;32(5):759–77.
- [20] Sobieszcanski-Sobieski J, Kodiyalam S, Yang R-J. Optimization of car body under constraints of noise, vibration, and harshness (NVH), and crash. AIAA paper no. 2000-1521, 2000.
- [21] Yang R-J, Gu L, Tho CH, Sobieszcanski-Sobieski J. Multidisciplinary design optimization of a full vehicle with high performance computing. AIAA paper no. 2001-1273, 2001.
- [22] Schramm U, Thomas H. Crashworthiness design using structural optimization. AIAA paper no. 98-4729, 1998.
- [23] Marklund P-O, Nilsson L. Optimization of a car body component subjected to impact. *Struct Multidisc Opt* 2001;21:383–92.
- [24] Fang H, Rais-Rohani M, Liu Z, Horstemeyer MF. A comparative study of metamodeling methods for multi-objective crashworthiness optimization. *Comput Struct* 2005;83(25–26):2121–36.
- [25] Jansson T, Redhe M, Nilsson L. Using surrogate models and response surfaces in structural optimization—with application to crashworthiness design and sheet metal forming. *Struct Multidisc Opt* 2003;25:129–40.

- [26] Eskandarian A, Kurtaran H, Marzougui D, Bedewi NE. Crashworthiness design optimization using successive response surface approximations. *Comput Mech* 2002;29(4–5):409–21.
- [27] Lee SH, Kim HY, Oh IS. Cylindrical tube optimization using response surface method based on stochastic process. *J Mater Process Technol* 2002;130–131:490–6.
- [28] Xiang YJ, Wang Q, Fan ZJ, Fang HB. Optimal crashworthiness design of a spot-welded thin-walled hat section. *Finite Elem Anal Des* 2006;42(10):846–55.
- [29] Yamazaki K, Han J. Maximization of the crushing energy absorption of tubes. *Struct Optim* 1998;16(1):37–46.
- [30] Lanzi L, Castelletti LML, Anghileri M. Multi-objective optimization of composite absorber shape under crashworthiness requirements. *Comput Struct* 2004;65(3–4):433–41.
- [31] Zarei HR, Kröger M. Multiobjective crashworthiness optimization of circular aluminum tubes thin-walled structures 2006;44(3):301–8.
- [32] Liu Y. Design optimisation of tapered thin-walled square tubes. *Int J Crashworthiness* 2008;13(5):543–50.
- [33] Hanssen AG, Langseth M, Hopperstad OS. Optimum design for energy absorption of square aluminium columns with aluminium foam filler. *Int J Mech Sci* 2001;43(1):153–76.
- [34] MATLAB user's guide and reference guide, The MathWorks Inc., 2009.
- [35] ANSA BETA-CAE systems, user's guide, Thessaloniki, Greece, 2008.
- [36] Wang B, Lu G. Mushrooming of circular tubes under dynamic axial loading. *Thin-Walled Struct* 2002;40:167–82.
- [37] Lu G, Yu T. Energy absorption of structures and materials. NW Boca Raton, FL, USA: CRC Press LLC; 2003.
- [38] Wang GG, Shan S. Review of metamodeling techniques in support of engineering design optimization. *ASME J Mech Des* 2007;129(4):370–80.
- [39] Currin C, Mitchell TJ, Morris MD, Ylvisaker D. Bayesian prediction of deterministic functions, with applications to the design and analysis of computer experiments. *J Am Stat Assoc* 1991;86(416):953–63.
- [40] Johnson ME, Moore LM, Ylvisaker D. Minimax and maximin distance designs. *J Stat Plan Infer* 1990;26(2):131–48.
- [41] Park JS. Optimal Latin-hypercube designs for computer experiments. *J Stat Plan Infer* 1994;39:95–111.
- [42] Taguchi G, Yokoyama Y, Wu Y. Taguchi methods: design of experiments. Allen Park, MI: American Supplier Institute; 1993.
- [43] Acar E, Rais-Rohani M. Ensemble of metamodels with optimized weight factors. *Struct Multidiscip Optim* 2009;37(3):279–94.
- [44] Myers RH, Montgomery DC. Response surface methodology: process and product optimization using designed experiments. New York: Wiley; 2002.
- [45] Buhmann MD. Radial basis functions: theory and implementations. New York: Cambridge University Press; 2003.
- [46] Simpson TW, Mauery TM, Korte JJ, Mistree F. Kriging models for global approximation in simulation based multidisciplinary design optimization. *AIAA J* 2001;39(12):2233–41.
- [47] Lophaven SN, Nielsen HB, Søndergaard J. DACE—a MATLAB kriging toolbox, informatics and mathematical modeling. Lyngby: Technical University of Denmark; 2002.